

## Clustering aspects in nuclear structure functions

M. Hirai,<sup>1</sup> S. Kumano,<sup>2</sup> K. Saito,<sup>1</sup> and T. Watanabe<sup>1</sup>

<sup>1</sup>*Department of Physics, Faculty of Science and Technology, Tokyo University of Science,  
2641, Yamazaki, Noda, Chiba, 278-8510, Japan*

<sup>2</sup>*KEK Theory Center, Institute of Particle and Nuclear Studies,  
High Energy Accelerator Research Organization (KEK)  
and Department of Particle and Nuclear Studies, Graduate University for Advanced Studies,  
1-1, Oho, Tsukuba, Ibaraki, 305-0801, Japan*

(Dated: December 28, 2010)

For understanding an anomalous nuclear effect experimentally observed for the beryllium-9 nucleus at the Thomas Jefferson National Accelerator Facility (JLab), clustering aspects are studied in structure functions of deep inelastic lepton-nucleus scattering by using momentum distributions calculated in antisymmetrized (or fermionic) molecular dynamics (AMD) and also in a simple shell model for comparison. According to the AMD, the  ${}^9\text{Be}$  nucleus consists of two  $\alpha$ -like clusters with a surrounding neutron. The clustering produces high-momentum components in nuclear wave functions, which affects nuclear modifications of the structure functions. We investigated whether clustering features could appear in the structure function  $F_2$  of  ${}^9\text{Be}$  along with studies for other light nuclei. We found that nuclear modifications of  $F_2$  are similar in both AMD and shell models within our simple convolution description although there are slight differences in  ${}^9\text{Be}$ . It indicates that the anomalous  ${}^9\text{Be}$  result should be explained by a different mechanism from the nuclear binding and Fermi motion. If nuclear-modification slopes  $d(F_2^A/F_2^D)/dx$  are shown by the maximum local densities, the  ${}^9\text{Be}$  anomaly can be explained by the AMD picture, namely by the clustering structure, whereas it certainly cannot be described in the simple shell model. This fact suggests that the large nuclear modification in  ${}^9\text{Be}$  should be explained by large densities in the clusters. For example, internal nucleon structure could be modified in the high-density clusters. The clustering aspect of nuclear structure functions is an unexplored topic which is interesting for future investigations.

PACS numbers: 13.60.Hb, 13.60.-r, 24.85.+p, 25.30.-c

### I. INTRODUCTION

Nuclear modifications of structure functions  $F_2$  were found by the European Muon Collaboration (EMC) [1], so that the phenomena is often called the EMC effect. Such modifications are now measured from relatively small  $x$  ( $\sim 10^{-3}$ ) to large  $x$  ( $x \sim 0.8$ ), where  $x$  is the Bjorken scaling variable. By using the data on nuclear structure functions, optimum parton distribution functions (PDFs) are proposed for nuclei [2, 3]. Physics mechanisms are different depending on the  $x$  region for producing the nuclear modifications. At small  $x$ , suppression of  $F_2$  occurs and it is known as nuclear shadowing. It is due to multiple scattering of a  $q\bar{q}$  pair coming from the virtual photon. At medium and large  $x$ , modifications are understood by conventional models mainly with nuclear binding and Fermi motion of nucleons. However, it may not be possible to explain full experimental modifications by such mechanisms, which indicates that internal structure of the nucleon could be also modified in a nuclear medium. For explanations of these physics mechanisms, the reader may look at Ref. [4].

In future, much details of the nuclear modifications will be investigated in lepton-nucleus deep inelastic scattering and hadron-hadron reactions. For example, a nuclear modification difference between up and down valence quark distributions ( $u_v$  and  $d_v$ ) will be investigated by measuring cross sections of semi-inclusive  $\pi^\pm$  productions [5]. It could lead to a possible solution of the long-

standing NuTeV weak-mixing angle ( $\sin\theta_W$ ) anomaly [6] from a viewpoint of the nuclear modification difference between  $u_v$  and  $d_v$  [7]. In addition, nuclear shell structure of the EMC effect, so called “local EMC effect” [8], will be investigated by measuring semi-inclusive reactions [9]. There is also an issue of the nuclear-modification difference between the structure functions of charged-lepton and neutrino reactions [10, 11]. It needs to be solved for a precise determination of nucleonic and nuclear PDFs. Such nuclear effects will be investigated by neutrino reactions of the MINER $\nu$ A project [12]. There will be also measurements at hadron facilities at RHIC (Relativistic Heavy Ion Collider), Fermilab (E906 experiment) [13], LHC (Large Hadron Collider), and possibly at J-PARC (Japan Proton Accelerator Research Complex) [14].

Measurements on the EMC effect at the Thomas Jefferson National Accelerator Facility (JLab) obtained an anomalous result for the beryllium-9 nucleus in comparison with measurements for other light nuclei [15]. It is anomalous in the sense that the magnitude of the nuclear-modification slope  $|d(F_2^A/F_2^D)/dx|$  is much larger in  ${}^9\text{Be}$  than the ones expected from its average nuclear density. From the experimental  ${}^9\text{Be}$  radius, namely the average nuclear density, modifications of  $F_2$  at medium  $x$  are expected to be much smaller than the ones of  ${}^{12}\text{C}$ , whereas measured values are similar in magnitude.

It is known in nuclear structure studies that the  ${}^9\text{Be}$  nucleus has a typical cluster-like structure rather than a shell-like one [16, 17]. It is like a cluster of two  $\alpha$

( ${}^4\text{He}$  nucleus) particles with surrounding neutron clouds according to the studies of antisymmetrized molecular dynamics (AMD). This fact indicates that there exist higher-density regions than the ones expected from the average density by the shell model or the one estimated by the experimental charge radius. The high-density regions could contribute to larger nuclear modifications of the structure function  $F_2$ . It could be a reason for the anomalous modification for  ${}^9\text{Be}$ . Such a cluster structure could produce high-momentum components in the momentum distribution of the nucleon, which is eventually reflected in modifications of quark momentum distributions, namely the structure functions of nuclei.

These considerations motivated us to investigate cluster aspects in the structure functions  $F_2^A$  for light nuclei, especially  ${}^9\text{Be}$ . At this stage, there is no theoretical work on the nuclear-clustering aspect in high-energy nuclear processes, for example, in structure functions, although there are some studies on multi-quark clusters such as a six-quark state in 1980's. Our current studies are totally different from these works on multi-quark effects. In this article, we investigate possible nuclear clustering effects on the structure functions  $F_2^A$  within a convolution model for describing  $F_2^A$  by using the AMD and shell-model wave functions.

In Sec. II, our theoretical formalism is provided for describing nuclear structure functions  $F_2^A$ . First, the convolution model is introduced. Then, the AMD description and a simple shell model are explained for calculating nuclear wave functions. In Sec. III, calculated nuclear densities are shown for  ${}^4\text{He}$  and  ${}^9\text{Be}$  in order to illustrate the clustering structure in the  ${}^9\text{Be}$  nucleus. Then, momentum distributions are shown for these nuclei. The ratios  $F_2^A/F_2^D$  are calculated in both AMD and shell models, and they are compared with experimental data. Finally, the nuclear modification slopes  $d(F_2^A/F_2^D)/dx$  are discussed. Our results are summarized in Sec. IV.

## II. FORMALISM

We explain a basic formalism for calculating the nuclear structure functions  $F_2^A$  in the convolution approach together with antisymmetrized molecular dynamics and a simple shell model for calculating nuclear wave functions. These models are somewhat obvious within each community in structure-function and nuclear-cluster physicists. However, the following introductory explanations are intended that different communities could understand with each other.

### A. Nuclear structure functions in convolution approach

The cross section of deep inelastic charged-lepton-nucleon (or nucleus) scattering is expressed by a lepton tensor  $L^{\mu\nu}$  multiplied by a hadron tensor  $W_{\mu\nu}$ :  $d\sigma \sim$

$L^{\mu\nu}W_{\mu\nu}$  [4, 18–20]. The hadron tensor is defined by

$$W_{\mu\nu}(p, q) = \frac{1}{4\pi} \int d^4\xi e^{iq \cdot \xi} \langle p | [J_\mu(\xi), J_\nu(0)] | p \rangle, \quad (1)$$

where  $q$  is the virtual photon four-momentum,  $p$  is the momentum of the nucleon (or nucleus), and  $J_\mu$  is the hadronic electromagnetic current. The hadron tensor  $W_{\mu\nu}$  is expressed by the imaginary part of the forward virtual Compton amplitude  $T_{\mu\nu}$  as  $W_{\mu\nu} = \text{Im}(T_{\mu\nu})/(2\pi)$  by the optical theorem.

The convolution model has been discussed in various articles within binding models for calculating nuclear structure functions, so that the detailed formalism should be found, for example, in Refs. [4, 19]. It indicates that a nuclear structure function is given by an integral of the nucleonic one convoluted with a momentum distribution of a nucleon in a nucleus as illustrated in Fig. 1. It is written in the hadron-tensor form as

$$W_{\mu\nu}^A(p_A, q) = \int d^4p_N S(p_N) W_{\mu\nu}^N(p_N, q), \quad (2)$$

where  $p_N$  and  $p_A$  are momenta for the nucleon and nucleus, respectively, and  $S(p_N)$  is the spectral function which is the energy-momentum distribution of nucleons in the nucleus. The structure functions are generally expressed in terms of two variables  $Q^2$  and  $x$  defined by

$$Q^2 = -q^2, \quad x = \frac{Q^2}{2M_N\nu}, \quad (3)$$

where  $M_N$  is the nucleon mass,  $\nu$  is the energy transfer  $\nu = q^0$  in the rest frame of a target nucleus, and  $q^2$  is given by  $q^2 = (q^0)^2 - \vec{q}^2$ . In the convolution picture of Eq. (2), the process is described by two steps as illustrated in Fig. 1. First, a nucleon is distributed in a nucleus according to the spectral function  $S(p_N)$  with the nucleon momentum  $p_N$ , and then a quark is distributed with the momentum fraction  $x$  in the nucleon. The overall quark momentum distribution is given by the convolution integral of these two distributions.

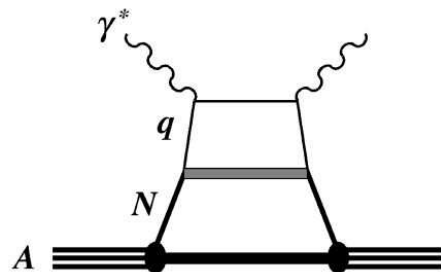


FIG. 1: Convolution approach for nuclear structure functions. The  $\gamma^*$ ,  $q$ ,  $N$ , and  $A$  indicate the virtual  $\gamma$ , quark, nucleon, and nucleus, respectively. A quark momentum distribution is described by the integral of a corresponding quark distribution convoluted with a nucleon momentum distribution.

The hadron tensor  $W_{\mu\nu}^A$  is expressed in terms of two structure functions  $W_1^A$  and  $W_2^A$  as

$$W_{\mu\nu}^A(p_A, q) = -W_1^A(p_A, q)\tilde{g}_{\mu\nu} + W_2^A(p_A, q)\frac{\tilde{p}_{A\mu}\tilde{p}_{A\nu}}{p_A^2}, \quad (4)$$

where  $\tilde{g}_{\mu\nu}$  and  $\tilde{p}_\mu$  are defined by  $\tilde{g}_{\mu\nu} = g_{\mu\nu} - q_\mu q_\nu / q^2$  and  $\tilde{p}_\mu = p_\mu - (p \cdot q) q_\mu / q^2$  so as to satisfy the current conservation. The structure function  $F_2^A$  is related to  $W_2^A$  by  $F_2^A = W_2^A p_A \cdot q / M_A$ , and its projection operator is given by [21, 22]

$$\hat{P}_2^{\mu\nu} = -\frac{M_A p_A \cdot q}{2\tilde{p}_A^2} \left( g^{\mu\nu} - \frac{3\tilde{p}_A^\mu \tilde{p}_A^\nu}{\tilde{p}_A^2} \right), \quad (5)$$

which satisfies  $\hat{P}_2^{\mu\nu} W_{\mu\nu}^A = F_2^A$ . The mass of the nucleus is denoted by  $M_A$ . Applying the projection operator on both side of Eq. (2), we obtain [4, 21, 23]

$$F_2^A(x, Q^2) = \int_x^A dy f(y) F_2^N(x/y, Q^2), \quad (6)$$

where  $F_2^A$  and  $F_2^N$  are structure functions for the nucleus and nucleon, and  $y$  is the momentum fraction

$$y = \frac{M_A p_N \cdot q}{M_N p_A \cdot q} \simeq \frac{A p_N^+}{p_A^+}, \quad (7)$$

where  $p^+$  is a light-cone momentum [ $p^+ \equiv (p^0 + p^3) / \sqrt{2}$ ]. It should be noted that the upper bound of the variables  $x$  and  $y$  is  $A$  for nuclei. The function  $f(y)$  indicates a light-cone momentum distribution for the nucleon, and it is given by

$$f(y) \equiv \frac{1}{A} \sum_i \int d^3 p_N y \delta \left( y - \frac{p_N \cdot q}{M_N \nu} \right) n_i |\phi_i(\vec{p}_N)|^2, \quad (8)$$

where  $n_i$  is the number of the nucleon in the quantum state  $i$ , and the summation is taken over the occupied states. Here, the spectral function is given by

$$S(p_N) = \frac{1}{A} \sum_i n_i |\phi_i(\vec{p}_N)|^2 \delta \left( p_N^0 - M_A + \sqrt{M_{A-i}^2 + \vec{p}_N^2} \right), \quad (9)$$

where  $M_{A-i}$  is the mass of residual one-hole state, and  $\phi_i(\vec{p}_N)$  is the wave function of the nucleon. Here,  $\vec{p}_N^2 / Q^2$ -type higher-twist effects [21] are not included in the convolution equation. The function  $f(y)$  is normalized so as to satisfy the baryon-number conservation  $\int_0^A dy f(y) = 1$  by taking  $\int dp_N^4 y S(p_N) = 1$  [23, 24].

The wave functions of the nucleon are calculated non-relativistically, and then they are used for the relativistic description in obtaining light-cone distributions by Eq. (8). It could lead to an issue of normalizing the non-relativistic wave function because there is no solid relativistic framework to use the non-relativistic functions. Here, the wave functions are normalized to satisfy the condition  $\int dy f(y) = 1$ , where there is an extra factor

of  $p_N^0 / M_N$  in front of  $|\phi(\vec{p}_N)|^2$ . As noticed in the third article of Ref. [25], this factor does not appear if a mass factor ( $M_N / p_N^0$ ) is included in the convolution formalism. However, such an overall normalization difference does not affect our results in Sec. III.

The separation energy  $\varepsilon_i$  is defined by

$$\varepsilon_i = (M_{A-i} + M_N) - M_A. \quad (10)$$

It is the energy required to remove a nucleon from the state  $i$ . In our actual calculation, we average over all the nucleons for estimating the average separation energy ( $\varepsilon_i \rightarrow \langle \varepsilon \rangle$ ). If a non-relativistic approximation is applied for the expression  $\sqrt{M_{A-i}^2 + \vec{p}_N^2}$ ,  $p_N^0$  and  $\langle \varepsilon \rangle$  are related by considering the  $\delta$  function for the energy conservation as

$$p_N^0 = M_N - \langle \varepsilon \rangle - \frac{\vec{p}_N^2}{2M_{A-1}}, \quad (11)$$

where  $M_{A-i}$  is replaced by  $M_{A-1}$  (the ground-state mass of the  $A-1$  nucleus). It should be noted that the residual nucleus  $A-i$  could be in an excited state and that many-body breakup processes could be also possible in the final state. Therefore, the separation energy is, in general, not a simple difference between the two nuclear binding energies in the initial and final states, since the final nucleus would not be in the ground state. It means that theoretical separation energies depend how they are estimated. For example, they vary depending whether models include short-range correlations [24, 26] and many-body breakup processes [27]. In our work, experimental separation energies are taken from  $(e, e'p)$  and  $(p, 2p)$  experiments.

Equation (6) indicates that the nuclear structure function  $F_2^A$  is split into two parts: the light-cone momentum distribution of the nucleon and the nucleonic structure function  $F_2^N$ . If there is no nuclear medium effect on the nucleonic structure function  $F_2^N(x, Q^2)$ , nuclear modifications should come solely from the nucleonic distribution part, which contains the information on nuclear binding and Fermi motion of nucleons. These effects are reflected in the light-cone momentum distribution of Eq. (8), namely in the momentum distribution of the nucleon and the energy-conserving  $\delta$  function. For calculating the distribution  $f(y)$ , we need a realistic model for the wave function  $\phi(\vec{p}_N)$ . In our work, we calculate it in two theoretical models: an antisymmetrized molecular dynamics and a simple shell model. They are introduced in Secs. II B and II C.

## B. Antisymmetrized molecular dynamics

This work is intended to investigate a possible clustering effect on the structure functions of deep inelastic scattering (DIS). There is a theoretical method, antisymmetrized molecular dynamics (AMD) [28] or fermionic molecular dynamics (FMD) [29], which is developed for

describing clustering aspects of nuclei as well as shell-like structure *on an equal footing*. Hereafter, we use the nomenclature AMD for this theoretical method.

There are nuclei which exhibit density distributions of separate clusters. For example, the  ${}^8\text{Be}$  nucleus has two separate peaks, which correspond to two  $\alpha$  nuclei, in its density distribution according to a Monte Carlo calculation for the eight-body system by using realistic  $NN$  ( $N$ : nucleon) potentials [30]. It suggests that some nuclei tend to form  $\alpha$ -like clusters within their structure since the  $\alpha$  is a tightly bound nucleus.

A simple and yet very useful and consistent theoretical method is provided by the AMD method. The AMD has a number of advantages, for example, that there is no assumption on nuclear structure, namely shell or cluster like configuration, and that simple and systematic studies are possible from light to medium-size nuclei. A nuclear wave function is given by the Slater determinant of single-particle wave packets:

$$|\Phi(\vec{r}_1, \vec{r}_2, \dots, \vec{r}_A)\rangle = \frac{1}{\sqrt{A!}} \det[\varphi_1(\vec{r}_1), \varphi_2(\vec{r}_2), \dots, \varphi_A(\vec{r}_A)] \\ = \frac{1}{\sqrt{A!}} \begin{vmatrix} \varphi_1(\vec{r}_1) & \varphi_1(\vec{r}_2) & \dots & \varphi_1(\vec{r}_A) \\ \varphi_2(\vec{r}_1) & \varphi_2(\vec{r}_2) & \dots & \varphi_2(\vec{r}_A) \\ \vdots & \vdots & \dots & \vdots \\ \varphi_A(\vec{r}_1) & \varphi_A(\vec{r}_2) & \dots & \varphi_A(\vec{r}_A) \end{vmatrix}. \quad (12)$$

Here, a nucleon is described by the single-particle wave function

$$\varphi_i(\vec{r}_j) = \phi_i(\vec{r}_j) \chi_i \tau_i, \quad (13)$$

where  $\chi_i$  and  $\tau_i$  indicate spin and isospin states, respectively. The function  $\phi_i(\vec{r}_j)$  is the space part of the wave function, and it is assumed to be given by the Gaussian functional form:

$$\phi_i(\vec{r}_j) = \left(\frac{2\nu}{\pi}\right)^{3/4} \exp\left[-\nu\left(\vec{r}_j - \frac{\vec{Z}_i}{\sqrt{\nu}}\right)^2\right], \quad (14)$$

where  $\nu$  is a parameter to express the extent of the wave packet. The center of the wave packet is given by  $\vec{Z}_i/\sqrt{\nu}$ . We should note that  $\vec{Z}_i$  is a complex variational parameter. Its real and imaginary parts indicate nucleon position and momentum, respectively [28]:

$$\frac{\langle \phi_i | \hat{r} | \phi_i \rangle}{\langle \phi_i | \phi_i \rangle} = \frac{\text{Re}\vec{Z}_i}{\sqrt{\nu}}, \quad \frac{\langle \phi_i | \hat{p} | \phi_i \rangle}{\langle \phi_i | \phi_i \rangle} = 2\sqrt{\nu} \text{Im}\vec{Z}_i. \quad (15)$$

A nuclear state is an eigenstate of the parity, so that the following parity-projected wave function is used:

$$|\Phi^\pm(\vec{r}_1, \vec{r}_2, \dots, \vec{r}_A)\rangle = \frac{1}{\sqrt{2}} \left[ |\Phi(\vec{r}_1, \vec{r}_2, \dots, \vec{r}_A)\rangle \pm |\Phi(-\vec{r}_1, -\vec{r}_2, \dots, -\vec{r}_A)\rangle \right]. \quad (16)$$

As for the  $NN$  interactions, we use the following potentials:

$$\begin{aligned} \text{2-body: } V_2 &= (1 - m - mP_\sigma P_\tau) \\ &\quad \times \left[ v_{21} e^{-(r/r_{21})^2} + v_{22} e^{-(r/r_{22})^2} \right], \\ \text{3-body: } V_3 &= v_3 \delta^3(\vec{r}_1 - \vec{r}_2) \delta^3(\vec{r}_2 - \vec{r}_3), \\ \text{LS: } V_{LS} &= v_{LS} \left[ e^{-(r/r_{LS1})^2} - e^{-(r/r_{LS2})^2} \right] \\ &\quad \times P(^3O) \vec{L} \cdot \vec{S}, \end{aligned} \quad (17)$$

where  $m$ ,  $v_{21}$ ,  $v_{22}$ ,  $r_{21}$ ,  $r_{22}$ ,  $v_3$ ,  $v_{LS}$ ,  $r_{LS1}$ , and  $r_{LS2}$  are constants. The two-body interaction part  $mP_\sigma P_\tau$  indicates the Majorana term with spin and isospin exchange operators ( $P_\sigma$ ,  $P_\tau$ ). The three-body part is a contact interaction form, and  $P(^3O)$  is the projection operator of the triplet-odd ( ${}^3O$ ) state (spin  $S=1$ , angular momentum  $L=\text{odd}$ ) in the two-nucleon system [31]. The Coulomb interaction is also considered in our analysis. The constants  $m$ ,  $v_{21}$ ,  $\dots$  are taken from Ref. [16] except for  $v_3$  and  $V_{LS}$ , which are fixed so as to reproduce binding energies of considered nuclei under the radius constraint:  $v_{LS} = 2000$  MeV,  $v_3 = 4000, 3300, 2000$  MeV for  ${}^4\text{He}$ ,  ${}^9\text{Be}$ ,  ${}^{12}\text{C}$ , respectively. Here, we should be careful to take into account the effect of center-of-mass motion [32].

The AMD wave functions contain the parameters  $\vec{Z}_i$  and  $\nu$ , which are determined by minimizing the system energy with a frictional-cooling method. Time development of  $\vec{Z}_i$  is described by the time-dependent variational principle:

$$\delta \int_{t_1}^{t_2} dt \frac{\langle \Phi(Z) | i \frac{d}{dt} - H | \Phi(Z) \rangle}{\langle \Phi(Z) | \Phi(Z) \rangle} = 0. \quad (18)$$

It leads to the equation of motion. Introducing two arbitrary parameters  $\lambda$  and  $\mu$  for practically solving the equation of motion, we obtain

$$i \frac{d}{dt} Z_i = (\lambda + i\mu) \frac{\partial H}{\partial Z_i^*}. \quad (19)$$

Here,  $\mu$  is a friction parameter which should be a negative number. By solving this equation, the parameters  $\vec{Z}_i$  are obtained. From the obtained parameters, the densities in coordinate and momentum spaces are calculated by

$$\rho(\vec{r}) = \left(\frac{2\nu}{\pi}\right)^{\frac{3}{2}} \sum_{i,j} \exp\left[-2\left(\sqrt{\nu}\vec{r} - \frac{\vec{Z}_i^* + \vec{Z}_j}{2}\right)^2\right] \\ \times B_{ij} B_{ji}^{-1}, \quad (20)$$

$$\rho(\vec{p}) = \left(\frac{1}{2\pi\nu}\right)^{\frac{3}{2}} \sum_{i,j} \exp\left[-\frac{1}{2}\left\{\frac{\vec{p}}{\sqrt{\nu}} - i(\vec{Z}_i^* - \vec{Z}_j)\right\}^2\right] \\ \times B_{ij} B_{ji}^{-1}, \quad (21)$$

where  $B_{ij} \equiv \int d\vec{r} \varphi_i^\dagger(\vec{r}) \varphi_j(\vec{r})$ . This momentum distribution is used for calculating the light-cone momentum

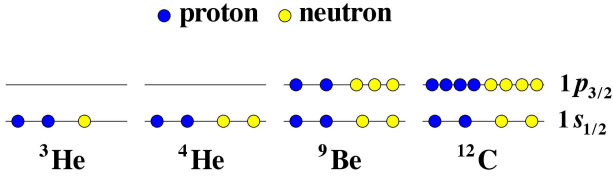


FIG. 2: (Color online) Shell levels for  ${}^3\text{He}$ ,  ${}^4\text{He}$ ,  ${}^9\text{Be}$ , and  ${}^{12}\text{C}$ .

distribution in Eq. (8). Then, using the convolution equation of (6), we obtain the nuclear structure functions, which include clustering effects described by the AMD.

### C. Simple shell model

In order to compare with the AMD results at this stage, we also calculate the nuclear spectral function by using a simple shell model, because the current wave functions and  $NN$  interactions in AMD are simple Gaussian forms. If much detailed studies become necessary in future, we may consider to use more sophisticated models, for example, a density-dependent Hartree-Fock [33] or a detailed shell model such as NuShell (OXBASH) [34].

As a shell model, we take a simple harmonic oscillator model. Nucleons are assumed to move in an average central potential created by interactions of all the nucleons in a nucleus. Then, the nucleons are treated independently with each other. A simple and yet realistic choice of the potential is the harmonic-oscillator type ( $M_N\omega^2 r^2/2$ ). Its wave function is separated into radial- and angular-dependent parts:

$$\psi_{n\ell m}(r, \theta, \phi) = R_{n\ell}(r)Y_{\ell m}(\theta, \phi), \quad (22)$$

where  $r$ ,  $\theta$ , and  $\phi$  are spherical coordinates, and  $n$ ,  $\ell$ , and  $m$  are radial, azimuthal, and magnetic quantum numbers, respectively. The function  $Y_{\ell m}(\theta, \phi)$  is the spherical harmonics, and the radial wave function is given by [35]

$$R_{n\ell}(r) = \sqrt{\frac{2\kappa^{2\ell+3}(n-1)!}{[\Gamma(n+\ell+1/2)]^3}} r^\ell e^{-\frac{1}{2}\kappa^2 r^2} L_{n-1}^{\ell+1/2}(\kappa^2 r^2), \quad (23)$$

where  $L_{n-1}^{\ell+1/2}(x)$  is the Laguerre polynomial, and  $\kappa$  is defined by  $\kappa \equiv \sqrt{M_N\omega}$ .

In the following analysis, the light nuclei,  ${}^3\text{He}$ ,  ${}^4\text{He}$ ,  ${}^9\text{Be}$ , and  ${}^{12}\text{C}$  are considered, so that the low-energy levels,  $1s_{1/2}$  and  $1p_{3/2}$ , are taken into account as shown in Fig. 2. The only parameter in the model is  $\omega$ , which is fixed by a nuclear radius. The constants of the AMD model are determined so as to explain experimental nuclear charge radii. Then, nuclear matter radii are calculated by using obtained AMD densities. Since it is the purpose of this work to investigate a difference between the structure functions of the AMD and shell models, we

take the constant  $\omega$  for each nucleus so as to obtain the same matter radius calculated by the AMD.

### D. Deuteron wave function

Experimental data are listed by ratios  $F_2^A(x)/F_2^D$ , where  $F_2^D$  is the structure function of the deuteron, for showing nuclear modifications in the structure functions. Since the deuteron is a bound two-nucleon system, a common wave function is used in Eq. (8) for calculating the structure function  $F_2^D(x, Q^2)$  of Eq. (6) in both AMD- and shell-model analyses. Here, we take the deuteron wave function given by the Bonn group in Ref. [36].

### E. Experimental information on separation energies, binding energies, and charge radii

In calculating the structure functions, experimental information is needed for separation energies, binding energies, and charge radii. The binding energies are taken from Ref. [37] and they are listed in Table I. They are used for calculating nuclear mass:  $M_A = Z M_p + N M_n - B$ , where  $M_p$  and  $M_n$  are proton and neutron masses,  $Z$  and  $N$  are atomic and neutron numbers, and  $B$  is the binding energy.

Experimental nuclear charge r.m.s. (root-mean-square) radii are listed for the deuteron [38],  ${}^3\text{He}$  [39],  ${}^4\text{He}$  [40],  ${}^9\text{Be}$  [41], and  ${}^{12}\text{C}$  [42] in Table I. Using these charge radii and binding energies, the constants in the AMD model are determined. The matter r.m.s. radii are then calculated in the AMD by using Eq. (20). There are slight differences between  $\sqrt{\langle r^2 \rangle_c}$  and  $\sqrt{\langle r^2 \rangle_m}$  in the AMD for  ${}^9\text{Be}$  and  ${}^{12}\text{C}$ . This is due to the effect of Coulomb force.

The separation energies are taken from experimental measurements for  ${}^4\text{He}$  [43],  ${}^9\text{Be}$  and  ${}^{12}\text{C}$  [44], and they are listed in Table I. A theoretical estimate 11.4 MeV is listed just for information because there is no available data for  ${}^3\text{He}$ . It was obtained by using a spectral function calculated by the Faddeev method with the Reid soft-core potential [45].

TABLE I: Experimental data for mean separation energies, binding energies per nucleon, and charge root-mean-square radii. The matter radii are calculated in the AMD model except for the deuteron so that charge radii agree with the data. The asterisk \* indicates a theoretical estimate of Ref. [45] because the experimental data is not available.

Nucleus	$\langle \varepsilon \rangle$ (MeV)	$B/A$ (MeV)	$\sqrt{\langle r^2 \rangle_c}$ (fm)	$\sqrt{\langle r^2 \rangle_m}$ (fm)
D	2.22	1.11	2.10	2.10
${}^3\text{He}$	(11.4*)	2.57	1.96	1.96
${}^4\text{He}$	20.4	7.07	1.68	1.68
${}^9\text{Be}$	24.4	6.46	2.52	2.61
${}^{12}\text{C}$	22.6	7.68	2.47	2.48

It should be also noted [46] that the separation energy 20.4 MeV of  ${}^4\text{He}$  [43] was obtained by using the data only in the peak region of the energy spectrum of  ${}^4\text{He}(p,2p){}^3\text{H}$  and a continuum region is not included. The separation energy should be calculated by the average energy weighted by the spectral function:

$$\langle \varepsilon \rangle = \int dE_N d^3p_N E_N S(E_N, p_N). \quad (24)$$

We notice that theoretical estimates are usually larger than this value (20.4 MeV) for  ${}^4\text{He}$  [26, 27]. For example, 28.2 MeV is obtained in Ref. [26], where the average kinetic energy estimated by the ATMS (Amalgamation of Two-body correlation functions into Multiple Scattering process) method is employed, and then the Koltun sum rule is used for estimating the separation energy  $\langle \varepsilon \rangle$ :  $B/A = [\langle \varepsilon \rangle - \langle T \rangle (A - 2)/(A - 1)]/2$ , where  $B/A$  is the binding energy per nucleon and  $\langle T \rangle$  is the average kinetic energy. However, it is very difficult to calculate a reliable value of the separation energy. The experimental separation energies  $\langle \varepsilon \rangle$  were obtained in nucleon-knockout reactions by observing peaks of single-particle excitations and they do not include the contribution from continuum states of the residual nucleus. Therefore, the mean separation energies would be underestimated. In this work, we estimated the clustering effect without the continuum, which needs to be considered in future for detailed comparison with data.

### III. RESULTS

First, nuclear densities are shown in the AMD model. The focused nucleus is  ${}^9\text{Be}$  for investigating the anomalous EMC effect in the structure function  $F_2$ , so that coordinate-space densities are shown in Fig. 3 for this  ${}^9\text{Be}$  nucleus as well as  ${}^4\text{He}$ , as an example, for comparison. It is interesting to find two density peaks within the  ${}^9\text{Be}$  nucleus, whereas the  ${}^4\text{He}$  density is a monotonic distribution. As mentioned in Sec. II, it is the advantage of the AMD method that it does not assume any specific structure, cluster- or shell-like configuration, on nuclei. The  ${}^4\text{He}$  is a tightly bound nucleus and it is well described by the usual shell-like structure, which is judged by the monotonic density distribution in Fig. 3. However, the situation is apparently different in  ${}^9\text{Be}$ . The figure suggests that two dense regions exist in  ${}^9\text{Be}$  although such a phenomenon does not exist in the shell model. It indicates that the  ${}^9\text{Be}$  nucleus consists of two  $\alpha$ -like clusters with surrounding neutron clouds. This clustering could produce different nuclear medium effects from the ones expected by the shell model. In particular, it could influence the nucleon momentum distribution, eventually quark momentum distributions, within the  ${}^9\text{Be}$  nucleus. Furthermore, dense regions could alter the internal structure of the nucleon.

Next, coordinate-space densities are compared in both AMD and shell models in Fig. 4 by taking averages over

the polar and azimuthal angles  $\theta$  and  $\phi$ . Although the  ${}^4\text{He}$  densities are same in both models, they are different in  ${}^9\text{Be}$ . Since the angular integrals have been done, the cluster structure is no longer apparent in the AMD density of  ${}^9\text{Be}$  in Fig. 4. However, the cluster effects are reflected in the slightly larger densities at  $r \sim 2$  fm and the depletion at  $r = 0$ , due to the existence of two separate clusters.

Instead of the coordinate-space density, the momentum-space density  $|\phi(\vec{p}_N)|^2$  is used for calculating the light-cone momentum distribution by Eq. (8). Calculated momentum-space densities are shown in Fig. 5 for the nuclei  ${}^4\text{He}$  and  ${}^9\text{Be}$ . We explained in Sec. IIE that the same radii are taken in both AMD and shell models. As a result, both momentum distributions of  ${}^4\text{He}$  are almost the same. However, the distributions are much different in  ${}^9\text{Be}$ . *It is important to find that the momentum distribution of the AMD is shifted toward the high-momentum region in  ${}^9\text{Be}$  because of the clustering structure.* This is caused by the fact that the dense regions, namely the two clusters, are formed within the  ${}^9\text{Be}$  nucleus. If nucleons are confined in the small space regions of the clusters, it leads to an increase of high momentum components, which is clearly shown in Fig. 5.

Now, using the obtained momentum distributions together with Eqs. (6), (8), and (9), we calculate the nuclear structure functions. The structure function of  ${}^9\text{Be}$  is

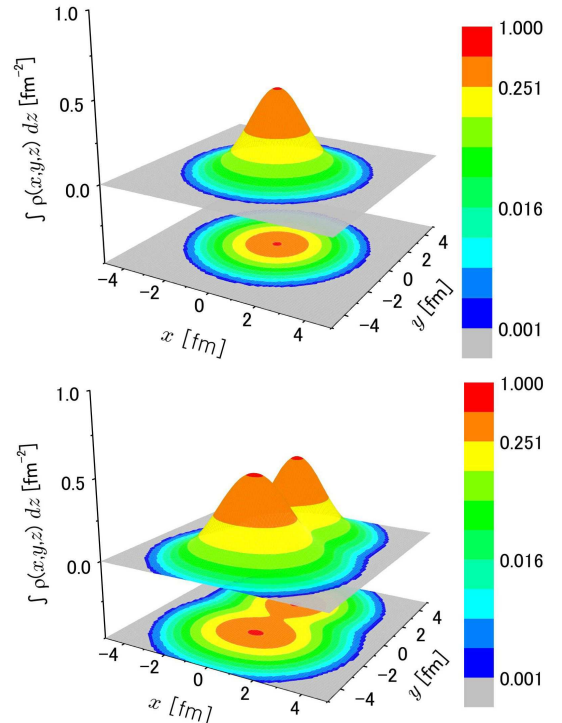


FIG. 3: (Color online) Upper and lower figures indicate coordinate-space densities of  ${}^4\text{He}$  and  ${}^9\text{Be}$ , respectively, calculated by the AMD. Here, the densities are shown by taking integrals over the coordinate  $z$ :  $\int dz \rho(x, y, z)$ .

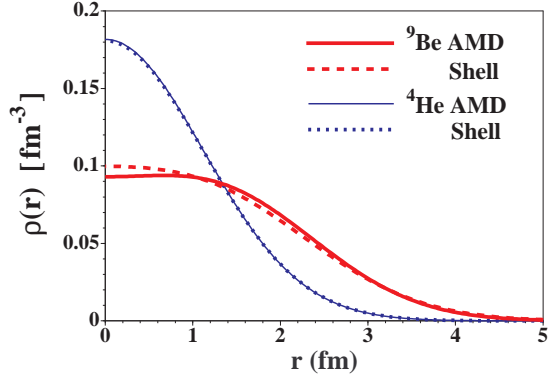


FIG. 4: (Color online) Coordinate-space densities are shown for  ${}^9\text{Be}$  ( ${}^4\text{He}$ ) in the AMD and shell models by the wide-solid (narrow-solid) and dashed (dotted) curves, respectively. The densities are integrated over the angles  $\theta$  and  $\phi$  for showing the curves in this figure. The clustering structure in the AMD gives rise to a modification of the density distribution in  ${}^9\text{Be}$ , whereas both densities are the same in  ${}^4\text{He}$ .

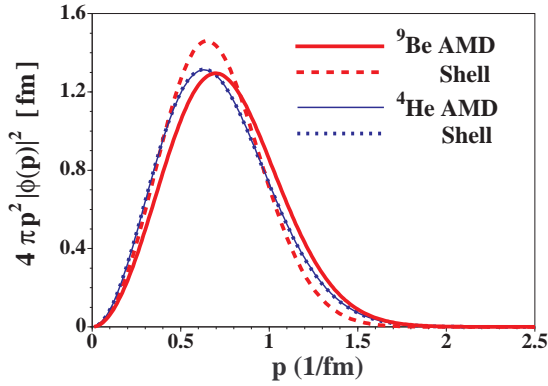


FIG. 5: (Color online) Momentum-space densities are shown for  ${}^4\text{He}$  and  ${}^9\text{Be}$  in the AMD and shell models. The clustering structure in  ${}^9\text{Be}$  gives rise to an excess of high-momentum components in the AMD.

shown together with the one of  ${}^4\text{He}$  as an example of non-cluster-like nuclei in order to illustrate clustering effects on the structure function of  ${}^9\text{Be}$ . In Figs. 6 and 7, our theoretical ratios  $F_2^{4\text{He}}/F_2^D$  and  $F_2^{9\text{Be}}/F_2^D$  are compared with the available experimental data of the SLAC (Stanford Linear Accelerator Center)-E139 [47], NMC (New Muon Collaboration) [48], and JLab [15]. The AMD and shell-model ratios are shown by the solid and dashed curves, respectively, and they are calculated at a fixed  $Q^2$  point ( $Q^2 = 5 \text{ GeV}^2$ ). Experimental data are taken at various  $Q^2$  points, and only the data with  $Q^2 \geq 1 \text{ GeV}^2$  are shown in Figs. 6 and 7. The JLab measurements include the data with small invariant mass  $W$ , where the process is not considered to be deep inelastic. Therefore, the data with  $W^2 < 3 \text{ GeV}^2$  are shown by the open circles. In showing the ratios of non-isoscalar ( $Z \neq N$ ) nuclei, isoscalar corrections are applied in Ref. [15] by including smearing corrections. Since we cannot access to the specific smearing corrections in the

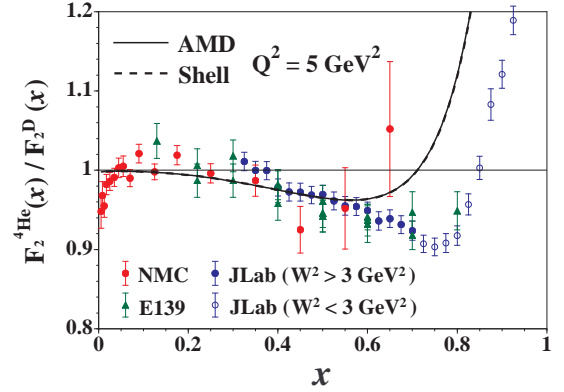


FIG. 6: (Color online) Theoretical structure-function ratios  $F_2^{4\text{He}}/F_2^D$  are compared with experimental data of SLAC-E139 [47], NMC [48], and JLab [15]. The solid and dashed curves indicate AMD and shell model results, respectively, calculated at  $Q^2=5 \text{ GeV}^2$ ; however, both curves overlap each other. The experimental data are taken at various  $Q^2$  points.

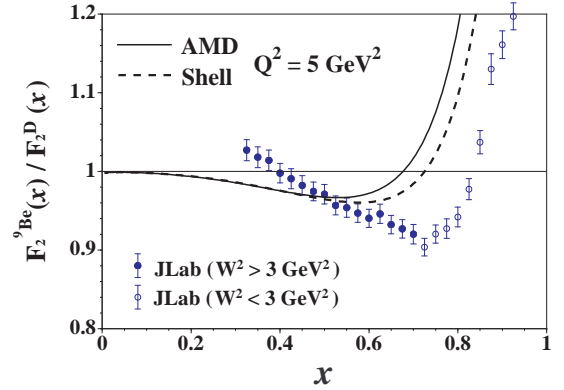


FIG. 7: (Color online) Comparison with JLab experimental data of  $F_2^{9\text{Be}}/F_2^D$ . Notations are the same as the ones in Fig. 6. The differences between the solid (AMD) and dashed (shell model) curves are now clear in  ${}^9\text{Be}$ . Isoscalar corrections are applied as explained in the main text.

JLab analysis, we simply used the isoscalar corrections  $[(F_2^p + F_2^n)/2]/[(ZF_2^p + NF_2^n)/A]$ , where  $F_2^p$  and  $F_2^n$  are the structure functions of the proton and neutron, respectively, by using the PDFs of the MSTW08 [11] in the leading-order (LO) of  $\alpha_s$ . We have checked that our corrections are almost the same as the corrections in the JLab analysis in  ${}^9\text{Be}$  [15].

From Figs. 6 and 7, we find that our theoretical ratios have a tendency consistent with the data in the sense that the ratio decreases at medium  $x$  and it increases at large  $x$ . These decrease and increase are caused by the nuclear binding and the nucleon's Fermi motion, respectively, in our convolution picture. However, it is also clear that the simple convolution description is not sufficient to explain the whole experimental nuclear modifications because there are differences between the theoretical curves and the data.

There are two major reasons for the differences. First,



short-range nucleon-nucleon correlations have not been included in calculating the spectral function [24, 26]. They change the theoretical ratios toward the experimental data at  $x = 0.6 - 0.8$ . The purpose of our studies is to investigate whether or not a possible clustering signature appears in deep inelastic lepton-nucleus scattering. Since this is the first attempt to investigate the cluster effects, we did not include such an effect. In future, we may consider to study more details.

Second, there could be a modification of nucleon itself inside a nuclear medium. As explained in Refs. [4, 19], such a nucleon modification was originally proposed as a  $Q^2$  rescaling model. Nucleons could overlap in a nucleus since the average nucleon separation and nucleon diameter are almost the same. The overlap then gives rise to a confinement radius change for quarks, which appears as a modification of quark momentum distribution, namely a modification of the structure function  $F_2$ . A possible internal nucleon modification was investigated in Refs. [49, 50] in comparison with the data. Since it is not the purpose of this work to step into such details, especially in comparison with the data, we leave it for our possible future studies.

The anomalous data was reported for  ${}^9\text{Be}$  by the JLab experiment [15] by taking a slope of the ratio  $F_2^A/F_2^D$  with respect to the Bjorken variable  $x$  in the region  $0.35 < x < 0.7$ . As shown in Fig. 4 of Ref. [15], the magnitude of the  ${}^9\text{Be}$  slope is too large to be expected from its average nuclear density in comparison with the ones of other light nuclei. We calculate corresponding theoretical slopes by taking the derivatives  $d(F_2^A/F_2^D)/dx$  ( $\equiv dR_{EMC}/dx$ ) at  $x = 0.35$ . The JLab data are plotted by the average density calculated by a Greens Function

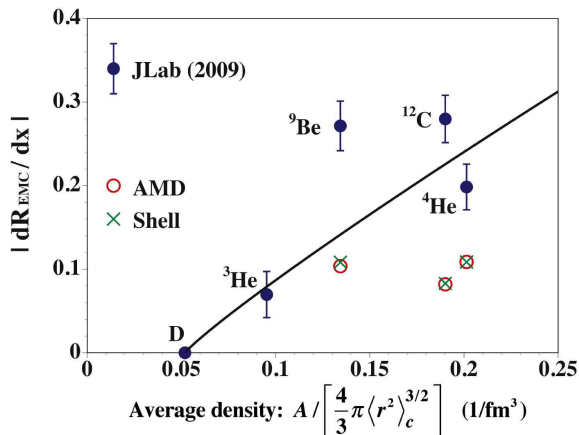


FIG. 8: (Color online) Comparison with JLab data on the slope  $|dR_{EMC}/dx|$ , where  $R_{EMC} = F_2^A/F_2^D$ . The open circles and crosses are the theoretical slopes calculated by the AMD and shell models, respectively. The JLab data are shown by the filled circles with errors. The abscissa is the average density  $\rho$  defined by  $A/[4\pi \langle r^2 \rangle_c^{3/2}/3]$  with the charge r.m.s. radius  $\sqrt{\langle r^2 \rangle_c}$ . The curve indicates a smooth function  $|dR_{EMC}/dx| = a(\rho - \rho_D)^b$  to fit the JLab experimental data except for  ${}^9\text{Be}$ .

Monte Carlo method [51] with the multiplication factor  $(A - 1)/A$  for removing the struck nucleon.

Although this theoretical density estimate would be reliable, we first show the slope by a purely experimental quantity by defining an average density as  $A/[4\pi \langle r^2 \rangle_c^{3/2}/3]$ , where  $\sqrt{\langle r^2 \rangle_c}$  is the experimental charge r.m.s. radius, in Fig. 8 instead of the specific theoretical density. The experimental charge radii are taken from Table I. The theoretical slopes in the AMD and shell models are shown by the open circles ( $\circ$ ) and crosses ( $\times$ ), respectively, for  ${}^4\text{He}$ ,  ${}^9\text{Be}$ , and  ${}^{12}\text{C}$ . Since the experimental separation energy is not available for  ${}^3\text{He}$ , the theoretical slopes are not calculated for  ${}^3\text{He}$ . The JLab data are shown by the filled circles with errors. In order to illustrate how the  ${}^9\text{Be}$  slope deviates from the other nuclear ones, a curve is given in Fig. 8 by fitting the data without the  ${}^9\text{Be}$  data in a simple functional form,  $|dR_{EMC}/dx| = a(\rho - \rho_D)^b$  where  $\rho = A/[4\pi \langle r^2 \rangle_c^{3/2}/3]$  and  $\rho_D$  is the density of the deuteron. The parameters  $a$  and  $b$  are determined and we obtain  $|dR_{EMC}/dx| = 1.35(\rho - \rho_D)^{0.906}$ , which is the curve in Fig. 8. It is obvious that the  ${}^9\text{Be}$  slope is anomalous in the sense that the data significantly deviates from the curve.

The magnitudes of the theoretical slopes are rather small in comparison with the data, and they are about half or less of the experimental ones in Fig. 8. This was already obvious from Figs. 6 and 7 that the magnitudes of the theoretical slopes are smaller than the experimental ones. As explained, the differences could be caused by the short-range correlations and internal nucleon modifications. An interesting result is that the clustering effects are not apparent in the slope by looking at both AMD and shell-model results for  ${}^9\text{Be}$  although there are some differences in the momentum distributions of Fig. 5 and in the structure functions of Fig. 7. In other nuclei, both theoretical slopes are almost identical. This is understood in the following way. In the medium- $x$  region, the nuclear modifications can be described mainly by the first two moments of the nucleon momentum distribution  $f(y)$ . These moments are expressed by the average separation and kinetic energies,  $\langle \varepsilon \rangle$  and  $\langle T \rangle$  [25], which are similar in both models. It leads to the small differences between the AMD and shell models in the slope  $dR_{EMC}/dx$ .

The small difference between the AMD and shell-model slopes in  ${}^9\text{Be}$  suggests us to look for another reason to explain the anomalous JLab data. As we noticed in Fig. 3, the high density regions are created locally in  ${}^9\text{Be}$  according to the AMD model. The higher densities could contribute to extra nuclear modifications in the structure function  $F_2^A$  by an additional mechanism which is not considered in our simple convolution picture. In order to find such a possibility, we plot the same slope by taking the maximum local density as the abscissa. The maximum density  $\rho_{max}$ , of course, depends on theoretical models to describe the nuclei. The maximum positions are located at  $r = 0$  for  ${}^4\text{He}$  in both AMD and shell mod-



els and also for  ${}^9\text{Be}$  in the shell model. However, they are at different points ( $r \neq 0$ ) for  ${}^9\text{Be}$  in the AMD due to the cluster structure and for  ${}^{12}\text{C}$  in both models due to a  $p$ -wave contribution to the density.

The slopes are shown in Fig. 9 by taking the maximum local density  $\rho_{max}$  as the abscissa. The maximum densities are almost the same in  ${}^3\text{He}$  and  ${}^4\text{He}$ , so that they are plotted at the same position of  $\rho_{max}$ . However, they differ in  ${}^9\text{Be}$  and  ${}^{12}\text{C}$ . Although the difference between  $\rho_{max}$  (AMD) and  $\rho_{max}$  (Shell) in  ${}^{12}\text{C}$  is not as large as the one in  ${}^9\text{Be}$ , it seems that there exist some clustering effects also in  ${}^{12}\text{C}$ . The JLab data of  ${}^9\text{Be}$  and  ${}^{12}\text{C}$  and the theoretical slopes are plotted at two different density points of the AMD and shell models. The curve indicates a fit to the JLab data with the  ${}^{12}\text{C}$  data at the shell-model density point by excluding the  ${}^9\text{Be}$  data. It is given by  $|dR_{EMC}/dx| = 0.821(\rho_{max} - \rho_{max_D})^{0.646}$ , where  $\rho_{max_D}$  is the maximum density for the deuteron.

In the usual convolution calculation, the spectral function is given by the averaged nuclear density distribution, and thus the inhomogeneity of the nuclear density is washed out. In such calculation, the average nuclear density of  ${}^9\text{Be}$  is lower than that of  ${}^{12}\text{C}$  or  ${}^4\text{He}$  as shown in Fig. 8, which is the origin of the “anomalous” EMC ratio of  ${}^9\text{Be}$  observed at the JLab. However, the maximum local density of  ${}^9\text{Be}$  is, as shown in Fig. 9, higher than that the ones of  ${}^4\text{He}$  and  ${}^{12}\text{C}$ , and the EMC ratio of  ${}^9\text{Be}$  can be treated “normally”. Here, the “normal” means that the result of  ${}^9\text{Be}$  is consistent with the smooth curve determined by the EMC results of other nuclei, and thus  ${}^9\text{Be}$  does not have anomalous dependence on the nuclear density anymore. In this sense, the anomalous  ${}^9\text{Be}$  result is “explained” as a normal one by the maximum local density; however, it does not mean that physics mechanism is clarified.

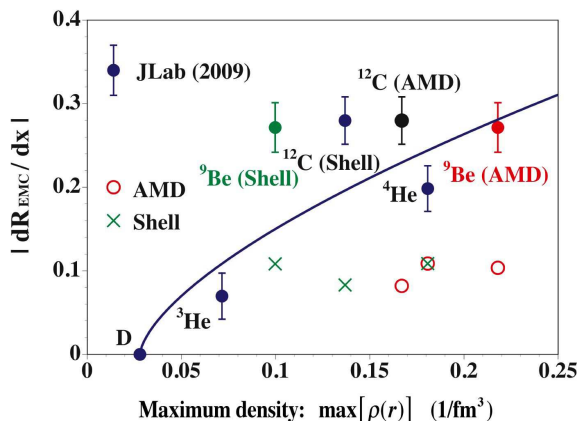


FIG. 9: (Color online) Comparison with JLab data on  $|dR_{EMC}/dx|$ . The abscissa is the maximum local densities theoretically calculated in the AMD and shell models. Two models produce different densities in  ${}^9\text{Be}$  and  ${}^{12}\text{C}$ , so that the JLab and theoretical slopes are plotted at different density points. The curve indicates a smooth function to fit the JLab experimental data except for  ${}^9\text{Be}$  with the  ${}^{12}\text{C}$  data at the shell-model density.

What we emphasize here is that the EMC ratio or the nuclear structure function itself could consist of the mean conventional part and the remaining one depending on the maximum local density. The remaining part is surely associated with the inhomogeneity of the nuclear density, before taking the average of nuclear wave function, given by the nuclear cluster structure. It could be nuclear-medium modification of the nucleonic structure function. It is well known that the cluster structure is well developed in Be and that the light mass region with  $A < 20$  is very suitable to study the cluster structure. Therefore, it is reasonable that, although the cluster-structure effect in the EMC ratio is not seen in the medium and large nuclei so far, we can now observe it in the beryllium isotope region. Such cluster structure will be investigated in the light-mass region by future JLab experiments [52].

It is interesting to find that *the “anomalous” JLab data for  ${}^9\text{Be}$  can be explained if it is plotted by the maximum local density at the cluster positions* because the  ${}^9\text{Be}$  (AMD) data is very close to the curve in Fig. 9. On the other hand, the  ${}^9\text{Be}$  data remains anonymous if it is plotted by the shell-model density because the  ${}^9\text{Be}$  (Shell) data significantly deviates from the curve. Such a tendency also exists in  ${}^{12}\text{C}$  but it is not as serious as the  ${}^9\text{Be}$  case. If the average nuclear density of  ${}^9\text{Be}$  is used in showing the slope data, the clustering effects are not clearly reflected. Here, it is important to point out that the  ${}^9\text{Be}$  data agrees with the other nuclear data if they are plotted as a function of the maximum density. This fact implies that *the physics mechanism associated with the high densities, for example due to the clusters in  ${}^9\text{Be}$ , could be the origin for explaining the nuclear-modification slopes of the  $F_2^A$  structure functions*. One of the possible mechanisms is the modification of internal nucleon structure caused by nuclear medium effects at the high density regions.

#### IV. SUMMARY

Nuclear modifications of structure function  $F_2$  were investigated for finding a possible signature of clustering structure in nuclei. The convolution model was used for describing nuclear structure functions, where momentum distributions of the nucleon were calculated in the AMD and shell models. According to the AMD, the  ${}^9\text{Be}$  nucleus has a clear clustering structure of two  $\alpha$ -like clusters with a surrounding neutron. Because of the cluster formation in  ${}^9\text{Be}$ , high-momentum components increase in the nuclear wave function of the AMD in comparison with the distribution of the shell-model one. Although there are some differences between the structure functions of  ${}^9\text{Be}$  in the AMD and shell models, the differences are rather small in our simple convolution picture. Therefore, an anomalous EMC effect found for  ${}^9\text{Be}$  at JLab should come from other effects such as the internal nucleon modification due to the high-density regions created by the clustering.

The following points are the major results in this work:

- (1) For the first time, the nuclear structure functions  $F_2^A$  are calculated in a model with clustering structure in nuclei. Then, they are compared with the structure functions of the shell model to clarify the clustering effects.
- (2) The clustering configuration in the  $^9\text{Be}$  nucleus produces high-momentum components in the nuclear wave function. It leads to a modification of the light-cone momentum distribution for nucleons in the  $^9\text{Be}$  nucleus.
- (3) Because of the high-momentum components due to the cluster formation, the nuclear structure functions  $F_2^A$  are modified; however, the modifications are not very large within the simple convolution description.
- (4) The anomalously large nuclear effect for the slope  $|d(F_2^A/F_2^D)/dx|$  of the  $^9\text{Be}$  nucleus observed at JLab can be explained if the slope is plotted by the maximum local density calculated in the theoretical model (AMD) with clustering structure.
- (5) Since the nuclear-modification slopes are explained by the maximum densities of nuclei, the physics mechanism of the anomalous nuclear effect could be associated with the high densities in the clusters of  $^9\text{Be}$ . This fact implies that internal nucleon modifications due to the high densities could be the origin of the  $^9\text{Be}$  anomaly, although careful estimations should be made on effects of short-range nucleon-nucleon correlations.

This work is the first attempt to connect the DIS structure functions to the clustering structure in nuclei. This kind of research field is an unexplored area, and further theoretical studies are needed for clarifying clustering effects in the structure functions.

#### Acknowledgments

The authors thank J. Arrington, C. Ciofi degli Atti, A. Daniel, A. Dote, D. Gaskell, N. Itagaki, H. Morita, T. Noro, N. Shimizu, and P. Solvignon for communications and suggestions.

- 
- [1] J. J. Aubert *et al.* (European Muon Collaboration), Phys. Lett. B **123**, 275 (1983).
  - [2] M. Hirai, S. Kumano, and M. Miyama, Phys. Rev. D **64**, 034003 (2001); M. Hirai, S. Kumano, and T.-H. Nagai, Phys. Rev. C **70**, 044905 (2004); **76**, 065207 (2007).
  - [3] K. J. Eskola, H. Paukkunen, and C. A. Salgado, JHEP **04**, 065 (2009) and references therein.
  - [4] D. F. Geesaman, K. Saito, and A. W. Thomas, Ann. Rev. Nucl. Part. Sci. **45**, 337 (1995).
  - [5] Jefferson Lab PAC-34 proposal, PR12-09-004 (2008).
  - [6] G. P. Zeller *et al.* (NuTeV Collaboration), Phys. Rev. Lett. **88**, 091802 (2002); Erratum **90**, 239902 (2003).
  - [7] S. Kumano, Phys. Rev. D **66**, 111301 (2002); M. Hirai, S. Kumano, and T.-H. Nagai, Phys. Rev. D **71**, 113007 (2005); K. J. Eskola and H. Paukkunen, JHEP **0606**, 008 (2006); I. C. Cloët, W. Bentz, and A.W. Thomas, Phys. Rev. Lett. **102**, 252301 (2009).
  - [8] S. Kumano and F. E. Close, Phys. Rev. C **41**, 1855 (1990); C. Ciofi degli Atti and S. Liuti, Nucl. Phys. A **532**, 235 (1991); C. Ciofi degli Atti, L. P. Kaptari, and S. Scopetta, Eur. Phys. J. A **5**, 191 (1999).
  - [9] C. Ciofi degli Atti, talk at the workshop on the Jefferson Laboratory Upgrade to 12 GeV, Seattle, USA, Oct. 27, 2009, <http://www.int.washington.edu/talks/WorkShops/int.09.3/>; K. Hafidi *et al.*, Jefferson Lab PAC-35, Letter of Intent (2009).
  - [10] I. Schienbein *et al.*, Phys. Rev. D **77**, 054013 (2008); M. Hirai, S. Kumano, and K. Saito, AIP Conf. Proc. **1189**, 269 (2009); H. Paukkunen and C. A. Salgado, JHEP **1007**, 032 (2010).
  - [11] A. D. Martin, W. J. Stirling, R. S. Thorne, and G. Watt, Eur. Phys. J. C **63**, 189 (2009). The LO PDFs are used in this work.
  - [12] For the MINERVA project, see <http://minerva.fnal.gov/>.
  - [13] E906 experiment at <http://p25ext.lanl.gov/e866/e866.html>.
  - [14] See <http://j-parc.jp/index-e.html> for the J-PARC project. S. Kumano, Nucl. Phys. A **782**, 442 (2007); AIP Conf. Proc. **1056**, 444 (2008).
  - [15] J. Seely *et al.*, Phys. Rev. Lett. **103**, 202301 (2009).
  - [16] Y. Kanada-En'yo, H. Horiuchi, and A. Ono, Phys. Rev. C **52**, 628 (1995).
  - [17] A. Dote, H. Horiuchi, and Y. Kanada-En'yo, Phys. Rev. C **56**, 1844 (1997).
  - [18] R. Devenish and A. Cooper-Sarkar, *Deep Inelastic Scattering* (Oxford University Press, 2004), pp. 57-60 & 370.
  - [19] R. G. Roberts, *The Structure of the Nucleon* (Cambridge University Press, 1993), pp. 8-12 & 144-153.
  - [20] S. Kumano, Phys. Rep. **303**, 183 (1998).
  - [21] M. Ericson and S. Kumano, Phys. Rev. C **67**, 022201 (2003).
  - [22] T.-Y. Kimura and S. Kumano, Phys. Rev. D **78**, 117505 (2008).
  - [23] G. L. Li, K. F. Liu, and G. E. Brown, Phys. Lett. B **213**, 531 (1988).
  - [24] C. Ciofi degli Atti, L. L. Frankfurt, L. P. Kaptari, and M. I. Strikman, Phys. Rev. C **76**, 055206 (2007).
  - [25] S. V. Akulinichev, S. A. Kulagin, and G. M. Vagradov, Phys. Lett. B **158**, 485 (1985); S. A. Kulagin, Nucl. Phys. A **500**, 653 (1989); S. A. Kulagin and R. Petti, Nucl. Phys. A **765**, 126 (2006).
  - [26] C. Ciofi degli Atti and S. Liuti, Phys. Rev. C **41**, 1100 (1990). See also C. Ciofi degli Atti and S. Simula, Phys. Rev. C **53**, 1689 (1996).
  - [27] H. Morita and T. Suzuki, Prog. Theor. Phys. **86**, 671 (1991).
  - [28] Y. Kanada-En'yo, M. Kimura, and H. Horiuchi, C. R. Physique **4**, 497 (2003); M. Kimura, A. Dote, A. Ohnishi, and H. Matsumiya, Genshikaku Kenkyu **53**, Supplement 2, 50 (2009) (in Japanese).
  - [29] H. Feldmeier and J. Schnack, Rev. Mod. Phys. **72**, 655

- (2000).
- [30] R. B. Wiringa, S. C. Pieper, J. Carlson, and V. R. Pandharipande, *Phys. Rev. C* **62**, 014001 (2000).
- [31] R. Tamagaki, *Prog. Theo. Phys.* **39**, 91 (1968).
- [32] A. Ono, H. Horiuchi, T. Maruyama, and A. Ohnishi, *Prog. Theo. Phys.* **87**, 1185 (1992).
- [33] P. Ring and P. Schuck, *The Nuclear Many-Body Problem* (Springer-Verlag, 2004).
- [34] See <http://knollhouse.org/>.
- [35] A. L. Fetter and J. D. Walecka, *Quantum Theory of Many-Particle Systems* (McGraw-Hill, 1971), pp. 508-511.
- [36] See pp.66-69 in R. Machleidt, K. Holinde, and C. Elster, *Phys. Rept.* **149**, 1 (1987).
- [37] G. Audi, A. H. Wapstra, and C. Thibault, *Nucl. Phys. A* **729**, 337 (2003).
- [38] R. C. Barrett and D. F. Jackson pp.146-147 in *Nuclear sizes and structure* (Oxford: Clarendon Press , 1977).
- [39] A. Amroun *et al.*, *Nucl. Phys. A* **579**, 596 (1994); J. Golak *et al.*, *Phys. Rep.* **415**, 89 (2005).
- [40] R. Roth *et al.*, *Nucl. Phys. A* **745**, 3 (2004).
- [41] F. Ajzenberg-Selove, *Nucl. Phys. A* **490**, 1 (1988).
- [42] H. De Vries, C. W. De Jager, and C. De Vries, *Atom. Data Nucl. Data Tabl.* **36**, 495 (1987).
- [43] H. Tyrén *et al.*, *Nucl. Phys.* **79**, 321 (1966).
- [44] S. Frullani and J. Mougey, *Adv. Nucl. Phys.* **14** (1984) 1. See page 194.
- [45] T. Uchiyama and K. Saito, *Phys. Rev. C* **38**, 2245 (1988).
- [46] H. Morita and T. Noro, personal communications (2010) on separation energies in  $^3\text{He}$  and  $^4\text{He}$ .
- [47] J. Gomez *et al.*, *Phys. Rev. D* **49**, 4348 (1994).
- [48] P. Amaudruz *et al.*, *Nucl. Phys.* **B441**, 3 (1995); M. Arneodo *et al.*, *ibid.* **B441**, 12 (1995).
- [49] K. Saito and A.W. Thomas, *Nucl. Phys. A* **574**, 659 (1994); I. C. Cloët, W. Bentz, and A. W. Thomas, *Phys. Lett. B* **642**, 210 (2006).
- [50] S. A. Kulagin and R. Petti, arXiv:1004.3062 [hep-ph].
- [51] S. C. Pieper and R. B. Wiringa, *Annu. Rev. Nucl. Part. Sci.* **51**, 53 (2001).
- [52] Jefferson Lab PAC-35 proposal, PR12-10-008 (2009).